Tutorial

Del Vecchio, A; Holobar, A; Falla, D; Felici, F; Enoka, R M; Farina, D

DOI:
10.1016/j.jelekin.2020.102426

Document Version
Peer reviewed version

Citation for published version (Harvard):
Del Vecchio, A, Holobar, A, Falla, D, Felici, F, Enoka, RM & Farina, D 2020, 'Tutorial: analysis of motor unit discharge characteristics from high-density surface EMG signals', *Journal of electromyography and kinesiology : official journal of the International Society of Electrophysiological Kinesiology*, vol. 53, 102426. https://doi.org/10.1016/j.jelekin.2020.102426

Tutorial: Analysis of motor unit discharge characteristics from high-density surface EMG signals

A. Del Vecchio[1], A. Holobar[2], D. Falla[3], F. Felici[5], R. M. Enoka[4], D. Farina[1]

Affiliations:

[1]Department of Bioengineering, Imperial College London, SW7 2AZ, London, UK.

[2]Faculty of Electrical Engineering and Computer Science, University of Maribor, Koroška cesta 46, 2000 Maribor, Slovenia

[3]Centre of Precision Rehabilitation for Spinal Pain (CPR Spine), School of Sport, Exercise and Rehabilitation Sciences, College of Life and Environmental Sciences, University of Birmingham, Birmingham, UK

[4]Department of Integrative Physiology, University of Colorado Boulder, Colorado

[5]Department of Movement, Human and Health Sciences, University of Rome "Foro Italico", Rome, Italy.

Corresponding author:

Dario Farina. Department of Bioengineering, Imperial College London, SW7 2AZ, London, UK. Tel: Tel: +44 (0)20 759 41387, Email: d.farina@imperial.ac.uk

Abbreviated title: Guidelines for surface EMG decomposition

Keywords: Motor units; Neural Drive; Blind source separation; Decomposition

Abstract

Recent work demonstrated that it is possible to identify motor unit discharge times from high-density surface EMG (HDEMG) decomposition. Since then, the number of studies that use HDEMG decomposition for motor unit investigations has increased considerably. Although HDEMG decomposition is a semi-automatic process, the analysis and interpretation of the motor unit pulse trains requires a thorough inspection of the output of the decomposition result. Here, we report guidelines to perform an accurate extraction of motor unit discharge times and interpretation of the signals. This tutorial includes a discussion of the differences between the extraction of global EMG signal features versus the identification of motor unit activity for physiological investigations followed by a comprehensive guide on how to acquire, inspect, and decompose HDEMG signals, and robust extraction of motor unit discharge characteristics.

Introduction

The generation of movement is accomplished by the transmission of synaptic inputs to motoneuron pools. The transducer of synaptic input into forces is the motor unit, which comprises a group of muscle fibres (muscle unit) and an alpha motor neuron. The neural information is transmitted by the motor unit through axonal action potentials (neural drive to the muscle) that elicit action potentials in the innervated muscle unit (motor unit action potentials, Figure 1). The summation and time-course of the motor unit action potentials determine the characteristics of the surface electromyogram (EMG) recorded with electrodes placed on the skin during motor tasks (Day and Hulliger, 2001; Fuglevand et al., 1992; Heckman and Enoka, 2012; Milner-Brown et al., 1973). The shapes of the surface-recorded motor unit action potentials are influenced by the properties of the volume conductor (Dimitrov and Dimitrova, 1974; Enoka and Duchateau, 2015; Farina et al., 2002b; Mañanas et al., 2016; Merletti et al., 2003; Stegeman et al., 1997).

Due to the physiological safety factor at the neuromuscular junction, the identification of motor unit action potentials from the interference EMG signals informs us about the discharge activity of individual motoneurons (Desmedt and Godaux, 1977; Duchateau and Enoka, 2011; Enoka and Duchateau, 2015; Gandevia et al., 1990; Henneman et al., 1965; Milner-Brown et al., 1973; Milner-Brown and Stein, 1975). Based on this approach, the motoneuron is the only nerve cell that can be noninvasively recorded in humans. For these reasons, several surface EMG decomposition methods have been proposed over the past three decades (Chen et al., 2018; Chen and Zhou, 2016; De Luca et al., 2006; Farina et al., 2010; Gazzoni et al., 2004; Holobar et al., 2014; Holobar and Zazula, 2007; Kumar et al., 2020; Nawab et al., 2010; Negro et al., 2016a). Of these methods, in this tutorial we focus exclusively on those based on blind source separation (BSS) methods applied to high-density surface EMG.

Over the past two decades, non-invasive high-density surface EMG (HDEMG) electrodes have been used to identify motor unit discharge times (Drost et al., 2001; Farina et al., 2002a; Gazzoni et al., 2005; Masuda and De Luca, 1991; Merletti et al., 2008, 1999; Zwarts and Stegeman, 2003). These recordings provide a spatial sampling of the motor unit action potentials at the skin surface (Holobar et

al., 2010; Merletti and Farina, 2016; Negro et al., 2016a; Zwarts and Stegeman, 2003). From these recordings, blind source separation (BSS) procedures can identify motor unit discharge times (Chen and Zhou, 2016; Holobar et al., 2010; Negro et al., 2016a) during a range of isometric tasks (A Del Vecchio et al., 2019c; Gallego et al., 2015; Martinez-Valdes et al., 2017). Although BSS decomposition procedures are performed in an automatic way, they require user-inspection of the identified motor unit spike trains (Enoka, 2019).

The aim of this tutorial article is to provide guidelines for the decomposition of HDEMG recordings. Moreover, we discuss the limits, the potential, and how to further validate the results obtained with HDEMG decomposition. The future advances needed in EMG decomposition are also discussed, with an emphasis on the computational challenges required to remove the subjectivity during visual editing of the motor unit spike trains.

1 – Extracting neural information from high-density EMG signals: Global EMG estimates vs. decomposition

Since the surface EMG signal is the algebraic summation of motor unit action potentials (Day and Hulliger, 2001), it is influenced by both the discharge times and the waveforms of the action potentials of the active motor units (Figure 1).

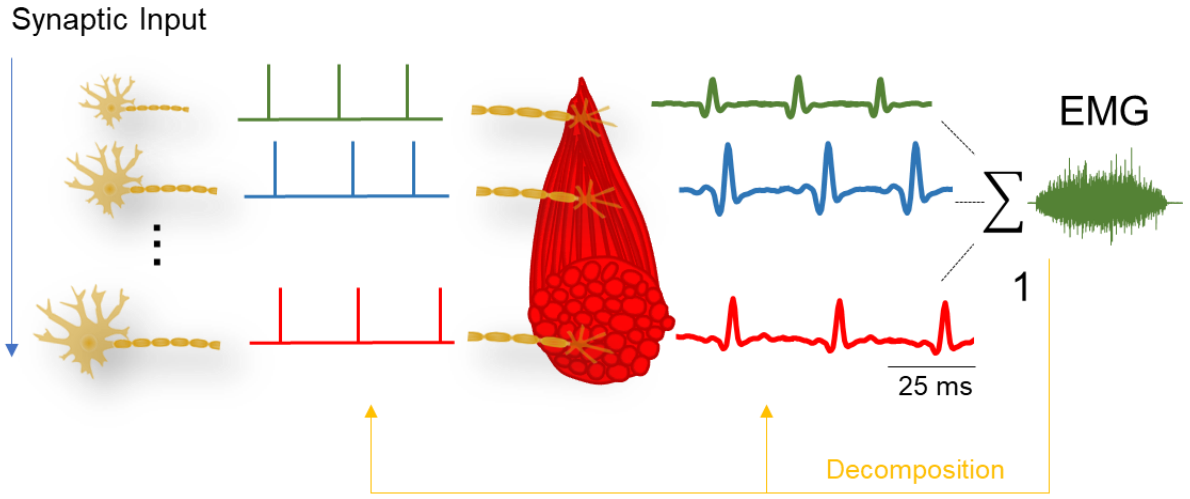

Figure 1 The one-to-one correspondence between axonal action potentials and motor unit action potentials. A pool of motoneurons discharges a series of action potentials (left) that are transformed by the muscle unit in a time series of motor unit action potentials (right). The motor unit action potential vary in amplitude and these differences are not always associated with the size of the motor unit, due to the influence of the volume conductor. The summation of the motor unit action potentials corresponds to the recorded EMG signals. Due to these effects, the association between the strength of the neural drive to the muscle and EMG amplitude is not always linear. Rather, the neural drive to the muscles can only be estimated from the motor unit discharge times, such as by decomposition of high-density surface EMG recordings (line 1 in orange). Conversely, conventional EMG analyses often estimate the neural drive to the muscle by extracting global features of the signal, such as amplitude or spectral moments. The decomposition of the EMG signal identifies the series of action potentials for individual motor units (red spikes). Due to several limitations with the global EMG, however, it is not always correct to infer the motoneuron population activity from global EMG signals, for example, because of the effects of amplitude cancellation and the non-linear relation between action potential sizes and recruitment thresholds. *Note that the innervation zones of the motoneurons are shown in largely different positions

of the muscle only to improve figure clarity while often the innervation zones are clustered in relatively small muscle portion.

The characteristics of the motor unit action potentials depend on many factors; for example, action potential amplitude and conduction velocity, which scale with the diameter of the muscle fibre (Håkansson, 1956; Plonsey and Barr, 1988). The amplitude of the motor unit action potentials also depends on the number of innervated muscle fibres, which is associated to the motor unit recruitment threshold (the voluntary force level corresponding to the first discharge of a motor unit) (Milner-Brown and Stein, 1975). However, this association is confounded by the influence of the volume conductor and, therefore, by the distance between the muscle fibres and the recording electrodes (Besomi et al., 2019) Consequently, the association between recruitment threshold and motor unit action potential amplitude is usually weak (Del Vecchio et al., 2017; Keenan et al., 2006), which influences the associations between EMG amplitude and the strength of the neural drive to the muscle and between EMG amplitude and force (Del Vecchio et al., 2017; Dideriksen et al., 2011; Fuglevand et al., 1993; Keenan et al., 2006; Komi and Viitasalo, 1976). It also makes it challenging to compare EMG amplitude across subjects, muscles, and time (Besomi et al., 2019).

Experimental results on the association between the amplitude of motor unit action potentials and motor unit size, which are consistent with simulation results of EMG generation (Farina et al., 2014), indicate that the amplitude of the EMG is only a crude indicator of the neural strategies used to control muscle force (Enoka, 2019; Enoka and Duchateau, 2015). Figure 2, for example, shows that the amplitude of the action potential waveforms for three motor units can be unrelated to the recruitment thresholds (Del Vecchio et al., 2017).

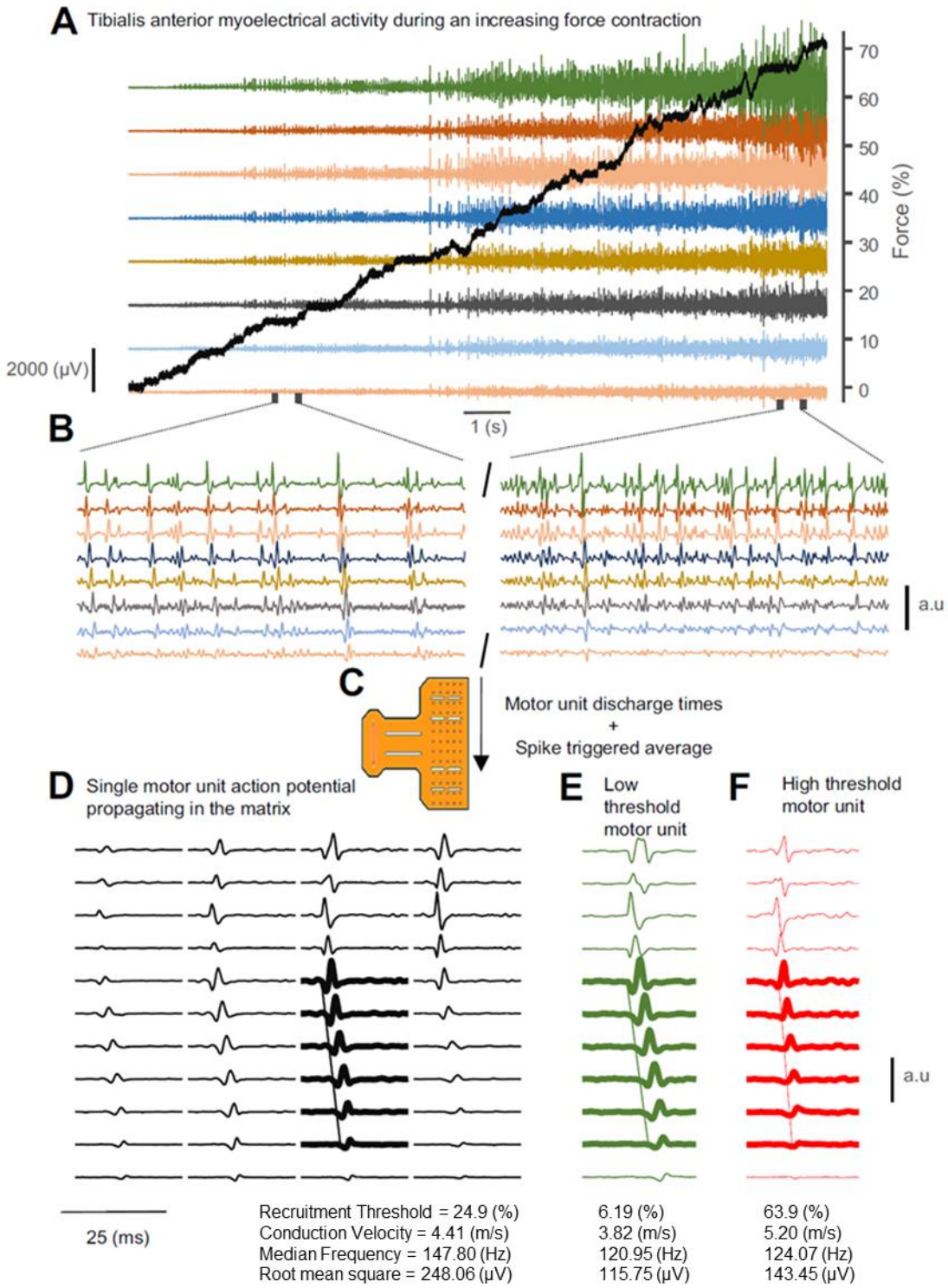

119

Figure 2 Association between motor unit action potential properties and recruitment threshold. **A** Eight double-differential EMG signals of the tibialis anterior muscle during an isometric ankle-dorsiflexion contraction at up to 70% of maximal voluntary force at a rate of 5% MVC/s (thick black trace). **B** 500 ms of EMG activity for the 8 channels. **C** Motor unit action potentials were identified by EMG decomposition and spike-triggered averaging. **D-E-F** Three representative motor unit action potentials with recruitment thresholds 24.9, 6.2, and 63.9 % of maximal force. The estimated conduction velocity, root mean square amplitude, and mean power spectral frequency are also shown for each motor unit action potential. (a.u = arbitrary units, scaled amplitude of the EMG). Reproduced with permission from Del Vecchio et al. (2017).

Contrary to surface action potential amplitude, the estimated conduction velocity of the motor unit action potentials has been shown to be associated with motor unit recruitment threshold across subjects and muscles, and to be influenced by different types of training interventions (Andreassen and Arendt-Nielsen, 1987; Casolo et al., 2019; Del Vecchio et al., 2017; Gazzoni et al., 2005; Martinez-Valdes et al., 2018; Masuda et al., 1996; Masuda and De Luca, 1991; Zwarts and Arendt-Nielsen, 1988). The conduction velocity estimated from the global EMG signal is the weighted average of the motor unit conduction velocities.

Due to the challenges associated with interpreting the features extracted from the surface EMG (Del Vecchio et al., 2017; Farina et al., 2014, 2004), intramuscular (LeFever et al., 1982; LeFever and De Luca, 1982; McGill et al., 2005; Stashuk and de Bruin, 1988) and surface EMG decomposition methods have been proposed (Chen et al., 2018; Chen and Zhou, 2016; De Luca et al., 2006; Farina et al., 2010; Gazzoni et al., 2004; Holobar et al., 2014; Holobar and Zazula, 2007; Nawab et al., 2010; Negro et al., 2016a). These methods identify individual motor unit action potentials during voluntary contractions and, therefore, allow the comparison of motor unit properties across subjects and time. Moreover, the same motor unit can be tracked over time (Del Vecchio and Farina, 2019; Martinez-Valdes et al., 2017) and compared across sessions including before and after training interventions (A Del Vecchio et al., 2019a; Martinez-Valdes et al., 2018). In contrast to global EMG analysis, the identification of the discharge times of individual motor units provides a direct estimate of the neural drive to muscle.

As an example of the information that can be obtained when decomposing EMG signals with respect to global analysis, we recently showed that the activity of motoneurons identified by EMG decomposition is predictive of the maximal rate of force development (A Del Vecchio et al., 2019c). Similarly, the detrimental influence of aging on force steadiness was shown to be associated with the variability in the common synaptic input to motoneurons, as estimated by EMG decomposition (Feeney et al., 2018).

Researchers now have a new tool to observe the neural code for movement in humans directly with a non-invasive approach that can be used in a variety of conditions. Nonetheless, surface EMG decomposition must be used carefully and requires expertise in signal acquisition, interpretation of results, and manual assessment of decomposition quality. After testing the validity of HDEMG decomposition algorithms in several methodological studies (e.g., Holobar *et al.*, 2010, 2014; Marateb *et al.*, 2011; Negro *et al.*, 2016*a*; Del Vecchio & Farina, 2019*a*), here we now share guidelines on how to perform HDEMG decomposition by BSS accurately and how to identify motor unit properties reliably.

2 - High-density surface EMG signals: acquisition

Prior to applying the high-density electrode grids (Figure 2C), the skin should be shaved, lightly abraded, and cleansed with an alcoholic solution and with abrasive paste (Piervirgili et al., 2014). Source separation is based on the assumption that action potential waveforms of motor units are unique when recorded by the grid. Therefore, the EMG electrodes should be placed in a location that assures maximal variations in shape of the action potentials of different motor units. For example, when recording from fusiform muscles, it is preferable to position the EMG array with its centre approximately

above a primary innervation zone. In other types of muscles (e.g., pennate muscles) the BSS is less sensitive to the position of the electrode array, although the electrodes will still need to be placed over the muscle belly. Interestingly, these requirements for decomposition are opposite to those often discussed for extracting global features from the EMG (Barbero et al., 2012).

The interelectrode distances used for HDEMG usually range from 3-4 mm to 10 mm (Drost et al., 2001; Merletti and Muceli, 2019; Zwarts and Stegeman, 2003; Del Vecchio et al., 2018; Farina et al., 2010; Feeney et al., 2018; Gazzoni et al., 2005; Holobar et al., 2010; Negro et al., 2016a). It should be noted that the electrode array does not need to satisfy the requirement for spatial Nyquist sampling frequency for successful BSS. Whether or not the spatial Nyquist criterion needs to be met depends on how the decomposition results will be used; for example, high spatial sampling may be necessary when analysing the spatial distribution of the identified motor unit action potentials (Merletti and Muceli, 2019). Therefore, the choice of the interelectrode distance is usually dictated by practical criteria, such as the size of the muscle.

After the electrode grids are applied, the signals should be assessed for quality. This should preferably be done by displaying the signals as monopolar recordings, as these signals are the most sensitive to interference. The visual inspection of monopolar signals allows the operator to find and remove the sources contaminating the recordings. The monopolar derivation is usually the most sensitive to signal interferences and therefore poses the highest constraints on signal quality, whereas the bipolar derivation better reveals the short-circuited EMG channels and also their spatial diversity. When the main sources of EMG signals are located at greater distances, it is not uncommon to observe EMG signals with high amplitudes in monopolar derivation but small amplitudes in bipolar derivation, because of the filtering of common spatial signal components by the bipolar system. In such cases, the spatial variation across different EMG channels is substantially reduced, effectively decreasing the number of useful EMG channels and, thus, the yield of BSS techniques. Accepted baseline noise levels for HDEMG signals are in the order of 10 – 40 μV RMS, but this requirement may vary with contraction intensity. From empirical experience, at low EMG amplitudes signal noise should be no more than one half of the power of the signal to ensure reliable decomposition (Del Vecchio et al., 2017; A Del Vecchio et al., 2019a). Aside from the electrode-skin and electronic-amplification noise (signal noise), EMG decomposition can only identify relatively few active motor units. The activity of the unidentified motor units is an additional, and often the main, source of noise for the decomposition process.

The EMG signals are usually band-pass filtered between 10-20 Hz at the low end and 400-500 Hz at the high end. This range keeps most of the EMG signal power while filtering out the contributions of signal noise. The decomposition process will be influenced by the choice of filter settings as this may alter the action potential waveforms. In general, the smaller the bandwidth, the greater the similarity of action potentials for different motor units. However, a smaller bandwidth does decrease the level of noise. The use of zero-phase filters, when possible, is recommended to avoid variable delays introduced for action potentials of different motor units and to keep the energy of motor unit action potentials concentrated in short intervals of time. Nonlinear filtering techniques change the EMG mixing model and should be avoided.

Noise may differ across channels and it may be necessary to remove some channels from the analysis. Among the methods that can be used to identify channels with low signal-to-noise ratio, one approach is to check the quality of the signal by estimating the power spectral density for each electrode in the grid and comparing it with the baseline. Figure 3 shows an example of 63 (from a total of 64) signals with high signal-to-noise ratio and shows how channels with poor signal quality can be identified. After having identified the electrodes showing high signal-to-noise ratio, potential power line interferences can be removed with filtering techniques (e.g., notch filters). Similar considerations apply for notch filters as for the choice of the bandpass filters discussed above.

After the EMG signal quality check, visual confirmation, and filtering of the EMG signals, the BSS decomposition can be initiated.

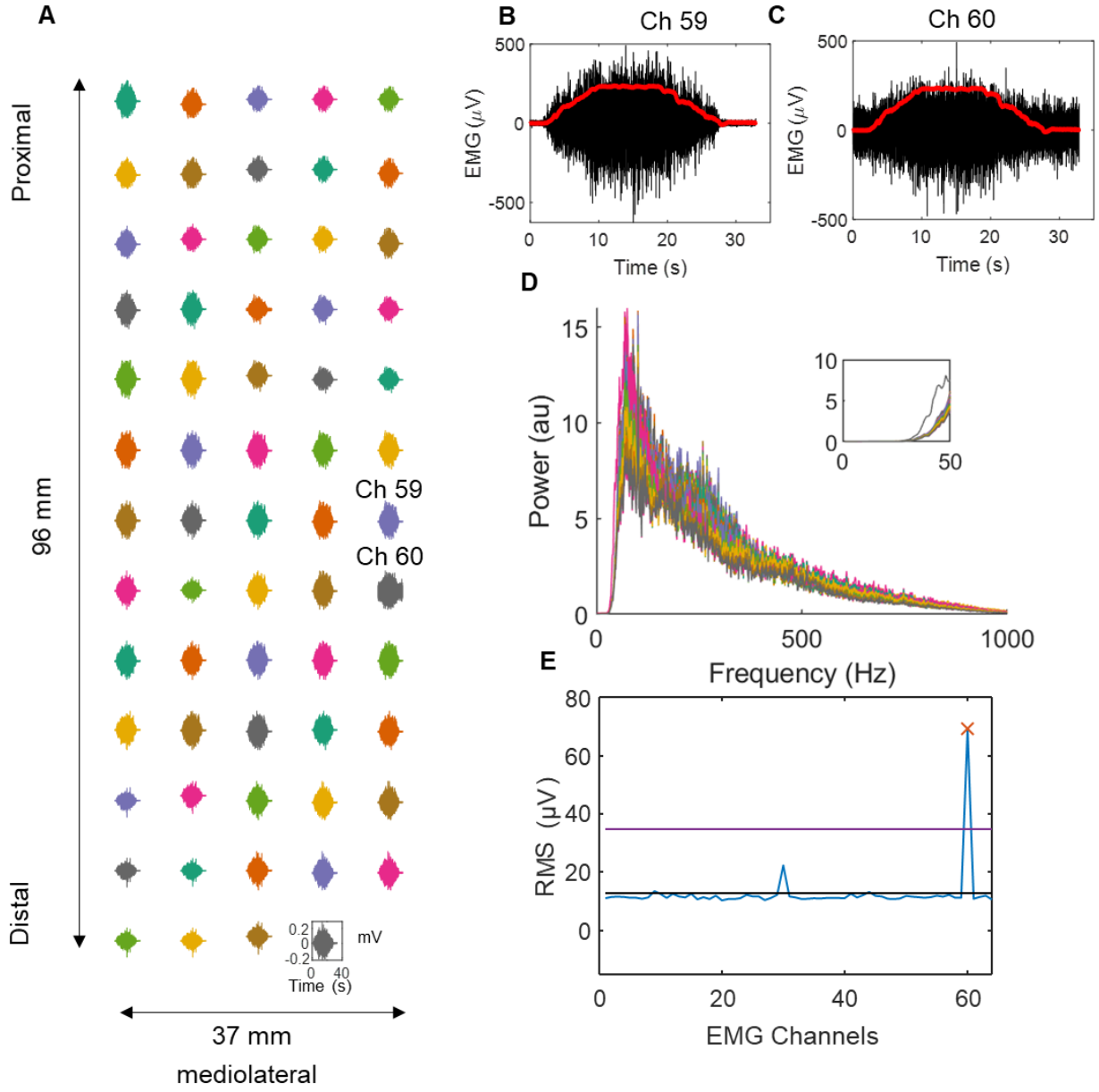

Figure 3 Example of detection and visual display of channels with poor signal-to-noise ratio. **A** Sixty-four monopolar EMG signals from the tibialis anterior muscle during a contraction at 35% of maximal

force. Two signals (channel 59 and 60) are highlighted and displayed in **B.** The force trace is indicated by the red lines. The 60th channel shown in **C** has a high level of noise at baseline, as it can be seen from its power spectral density (**D**) and from the baseline amplitude of the EMG. **D.** The power spectral density of each of the 64 channels, as computed from the full contraction duration (~24 s). Note that one channel (in the inset, grey line) shows higher power at lower frequencies than all the others. This indicates poor signal-to-noise ratio (channel 60, au for auxiliary units) **E.** Three standard deviations from the EMG root mean square (RMS) baseline across the grid shows the outlier channel.

3 - High-density surface EMG signals: decomposition

High-density EMG signals are decomposed into individual motor unit action potentials with methods that have limited a-priori information. Figure 4 shows an overview of the decomposition process: acquisition of HDEMG recordings, separation of sources (motor units) via BSS, visual inspection, and raster plot of the reliably identified motor units. BSS procedures usually estimate one motor unit spike train at a time by iteratively optimizing the motor unit separation filter and applying it to the recorded EMG signals. Importantly, optimization of the motor unit filter builds on a measure of sparseness for the motor unit spike train based on a predefined time interval. Different measures of spike-train sparseness have been proposed (Chen and Zhou, 2016; Holobar and Zazula, 2007; Negro et al., 2016a), but they all require relatively long EMG recordings for the spike train to be estimated reliably. Consequently, current BSS algorithms should be applied to EMG signals that last at least 5 s.

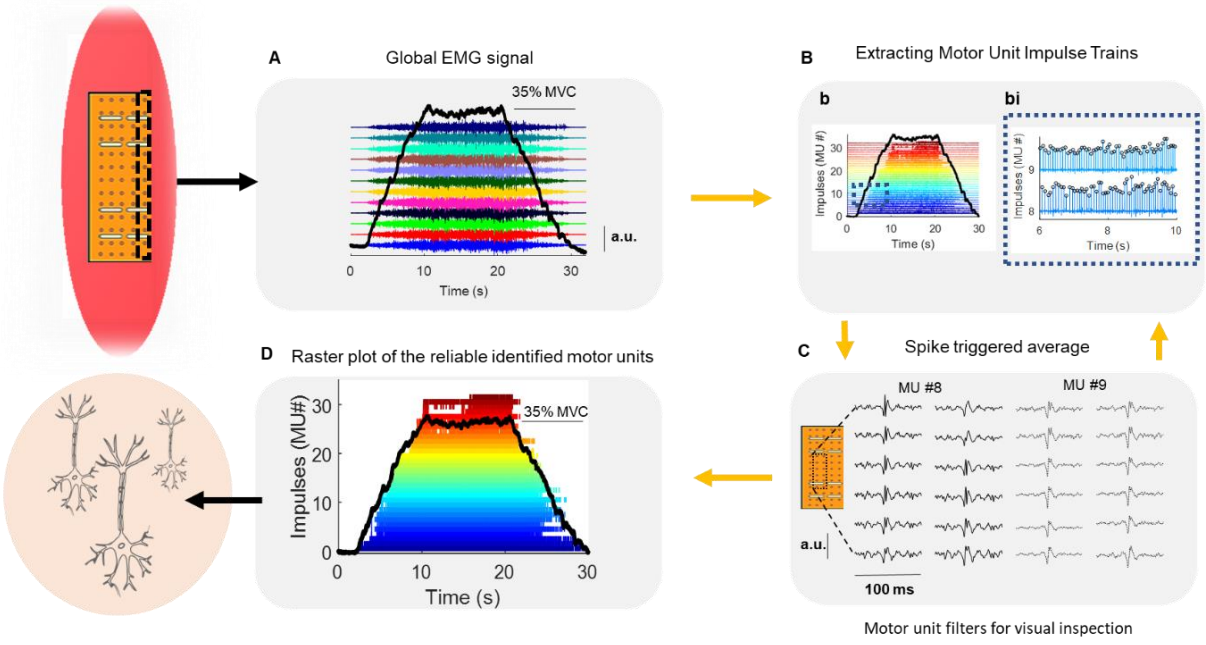

Figure 4 Example of high-density surface EMG decomposition with blind-source separation and visual inspection of the signals. **A**. Tibialis anterior monopolar EMG activity during an isometric contraction. The rate of force development was 5% MVC/s with a plateau phase of 10 s. One column of the high-density EMG grid (64 electrodes in total, with 8 mm of interelectrode distance, au arbitrary units) is shown color-coded. Specifically, the channels highlighted by the dotted black trace (over the muscle, left side of the figure) are shown in **A**. In this example, the signal-to-noise ratio is similar for all 64 electrodes in the matrix. **B.** Extraction of motor unit pulse trains by blind-source separation. The 64 channels are decomposed blindly, and the output of the algorithm are impulse trains with heights corresponding to the weights of the motor unit action potential shapes in the matrix obtained by the

independent component analysis process. The two insets in B (b and bi) show the motor unit impulses extracted by blind-source separation for each motor unit. The next iteration is to check each motor unit action potential visually, as shown in **bi**, and reiterate the source separation manually by triggering the motor unit action potential in a fixed time window, usually in the order of 3-5 s, as shown in **bi** and **C**. After visual inspection of all the motor unit spike trains, it is possible to observe the raster plot of all identified motor units (**D**). The motor unit waveforms in **C** represents the motor unit waveforms corresponding to 12 electrodes after spike-triggered averaging.

4 - High-density surface EMG signals: visual inspection of decomposition results

Due to the sparseness of the motor unit spike train, BSS calculates the motor unit separation filter from those time instants in the EMG recording when the motor unit was likely to be active. Once the motor unit spike train is identified, the motor unit filter can be re-calculated based only on the identified motor unit spikes, in an iterative way. This can be accomplished by inspecting the results of the BSS algorithm, so that the operator can manually identify and remove from the calculation of the separation filter the spikes of lower quality. Note that this partly manual selection is for the calculation of the separation filter only and not for the output of the decomposition (see also below). This selection can often improve the motor unit separation filter estimates beyond the level achieved by the BSS algorithm used fully automatically. For example, when decomposing EMG signals that contain artefacts, the BSS algorithm will try to optimize the motor unit filter on all the motor unit spikes, including those occurring concurrently with artefacts. It is exactly this noise and the residual activity of the other motor units that is measured by some signal-based metrics of accuracy, such as the pulse-to-noise ratio (Holobar et al., 2014).

Under assumption of nonstationary noise and artefacts, following the initial automatic decomposition it is always possible to identify the portions of a spike train with low pulse-to-noise ratio and exclude those portions from the motor unit filter calculation. It is not a simple matter to implement the exclusion of the low-quality portions of the motor unit spike train automatically in a BSS algorithm. Indeed, the pulse-to-noise ratio (and therefore the quality of spike train portions) may change due to many factors such as the contraction level (increase of contraction level increases the contributions of other motor units), changes of skin-electrode contact noise, instrument noise, and signal artefacts. The human operator builds on the knowledge of the experimental protocol and currently can decide which signal intervals to exclude from the motor unit filter optimization better than a BSS algorithm, which has no knowledge on the experimental conditions.

After exclusion of spike-train intervals with poor signal quality, the motor unit filter should be re-calculated and re-applied to the entire EMG signal in order to re-estimate (objectively, without any manual intervention) the entire motor unit spike train. An example of this procedure if shown in Figure 5.

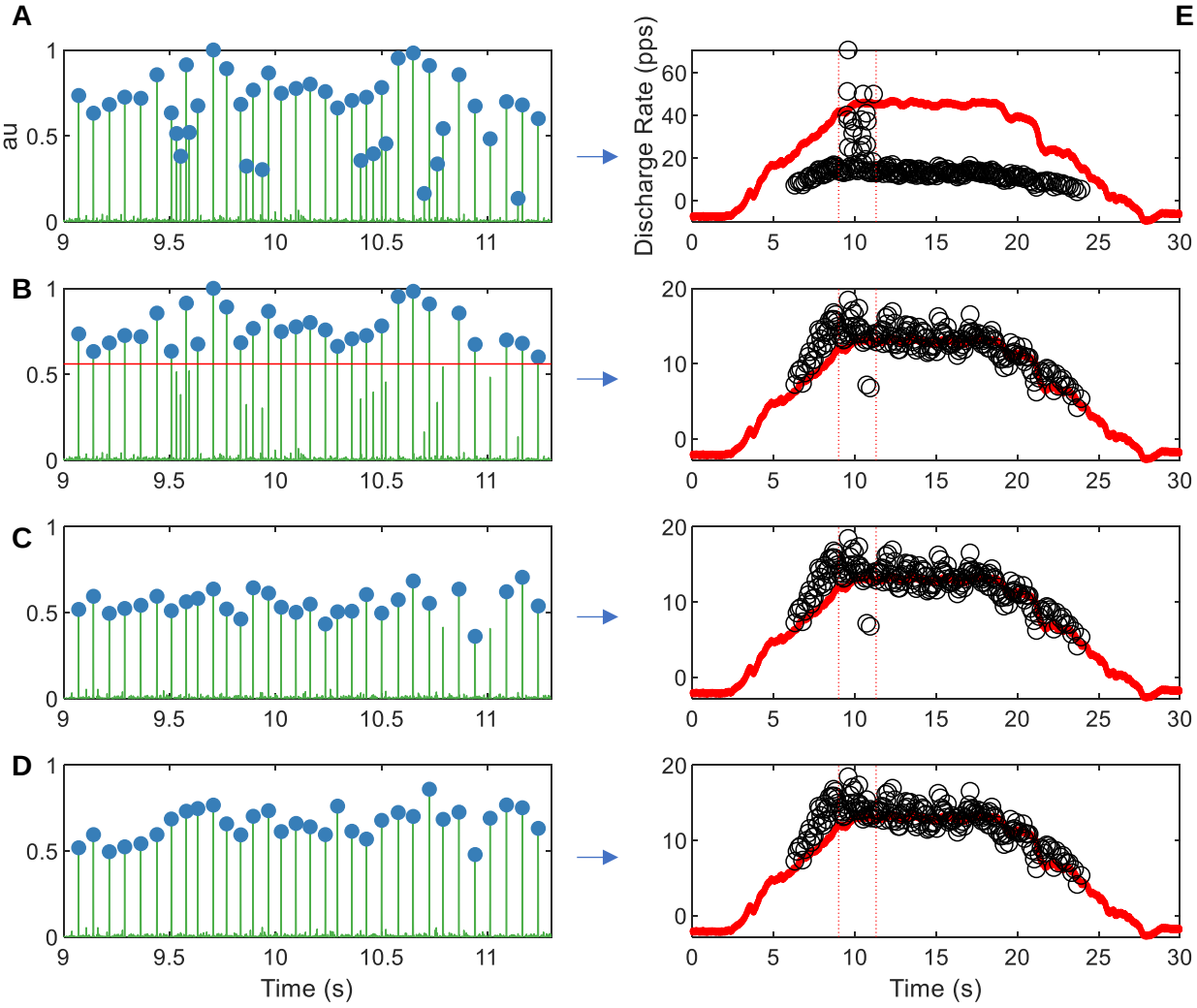

Figure 5. Visual reiterations of the motor unit discharge times identified by blind source separation (**A-D**). The blind source separation automatically identified the discharge times of a motor unit. In **A**, the left plot depicts the identified spike train with many spikes below the average spike height. Automatically identified motor unit firings are depicted by blue circles. The discharge times of the motor unit (right plot) show a strong mismatch with the average motor unit discharge rate and force trace in red. In these instances, a time window of ~3 s is centred in the location of interest (red dashed lines in **E**). Within this location, the motor unit filter is reconstructed after removing the firings below a certain threshold, as depicted in **B.** The motor unit filter is then reapplied to the HDEMG signals, yielding a new spike train estimate that is depicted in **C**. Afterwards, two more spikes are recognized as motor unit firings and manually added in **D.** In this way, the motor unit filter that was identified by blind source separation is visually edited and yields a robust estimate of the motor unit firings.

Manual exclusion of spike-train intervals in manual optimization of the motor unit filter may or may not rely on the human knowledge of motor unit firing regularity. Although this additional information may be beneficial, it may also bias the selection of motor unit spikes that are taken into consideration when manually re-calculating motor unit filters. Importantly, manual spike selection should only be used for motor unit filter optimization. Afterwards, manually optimized motor unit filters should be applied to the entire EMG signal and objective spike segmentation procedures need to be followed to discriminate spikes from baseline noise in the identified motor unit spike train. Subjective selection of motor unit spikes in the final motor unit spike train (final decomposition result) should be avoided as it may lead to biasing the decomposition results.

5 - High-density surface EMG signals: decomposition accuracy

The extraction of motor unit action potentials from high-density EMG signals has been extensively validated, but mainly during isometric contractions. The current accepted approach for the validation of surface EMG decomposition is a variant of the two-source method previously introduced by Mambrito & De Luca (1984) for intramuscular EMG decomposition. With this method, intramuscular and HDEMG signals are concurrently recorded and the results of their decomposition compared (Holobar et al., 2014, 2010; Hu et al., 2014; Marateb et al., 2011). Figure 6 shows a raster plot of motor units concurrently identified from surface and intramuscular signals, with the respective accuracies.

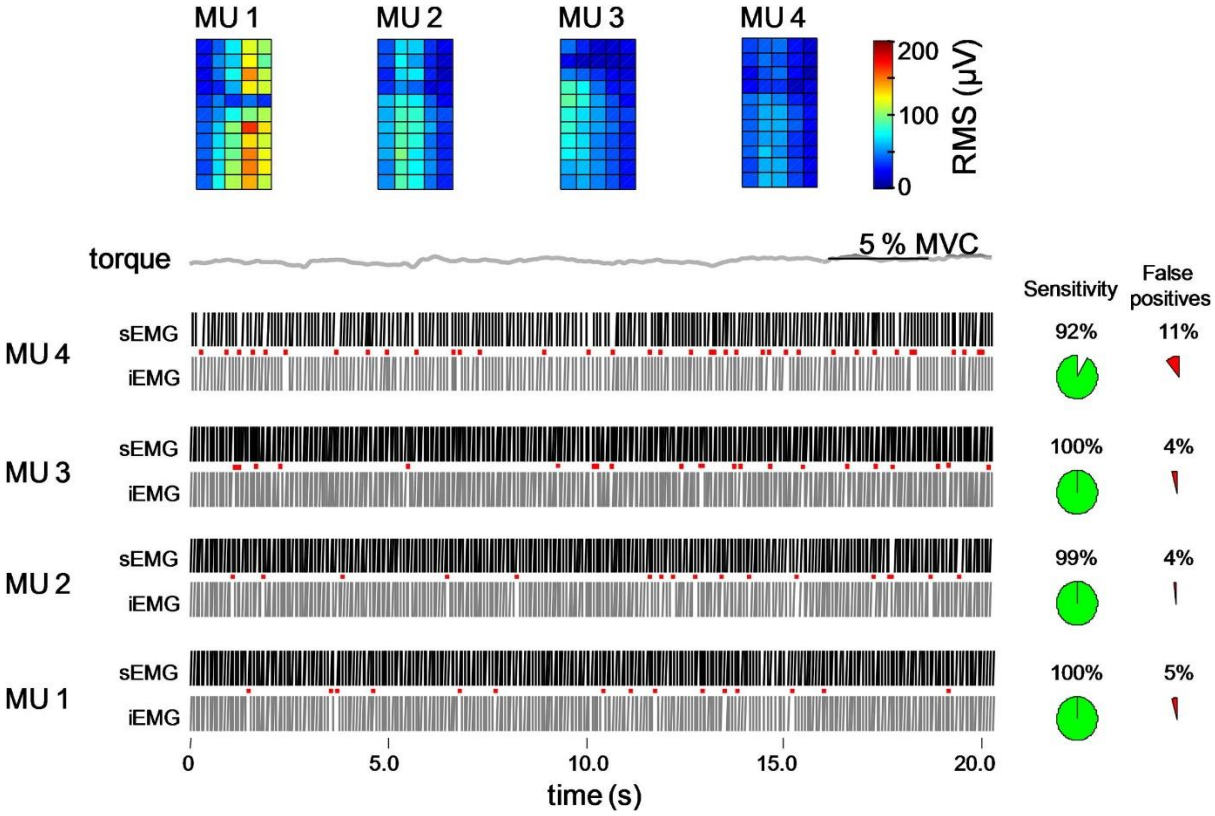

Figure 6 Two-source method to assess accuracy. The intramuscular electromyogram(iEMG) is recorded concurrently with high-density surface EMG (sEMG) from the abductor digiti minimi muscle at 5% of the maximal voluntary contraction. The sensitivity and false positive rate for discharge time

identification are computed by comparing the output of intramuscular and surface EMG decomposition. In this example, the bottom raster plot shows the motor unit discharge times that were identified from the intramuscular EMG signal decomposition and, at the top, those identified by blind-source separation of the HDEMG signals. The top plot in each pair shows the distribution of amplitude of the motor unit action potential waveforms over the high-density EMG grid. The sensitivity of the high-density EMG (right) represents the number of discharge times that are concurrently identified by the surface and intramuscular EMG decomposition divided by the total number of discharges identified from the intramuscular EMG. The percent of false positives corresponds to the number of discharges identified by the surface but not by the intramuscular EMG decomposition, divided by the total number of discharges identified from the intramuscular EMG. MU, motor unit. Reproduced with permission from Farina et al. 2010.

Indirect methods of validating surface EMG decomposition use shape analysis of two-dimensional motor unit action potentials identified by BSS (Del Vecchio and Farina, 2019; Hu et al., 2015, 2013a; Thompson et al., 2018) and simulation approaches (Farina et al., 2010; Holobar and Zazula, 2007). For example, accuracy measures, such as pulse-to-noise ratio (Holobar et al., 2014), the silhouette measure (Negro et al., 2016a), or the motor unit action potential similarity after spike-triggered averaging (see below) across the contractions with or without injection of gaussian noise (Del Vecchio and Farina, 2019; Thompson et al., 2018), can be used to infer the accuracy of motor unit spike identification. All of these measures are asymptotic and increase their precision with the number of identified spikes in the spike train. Therefore, they should not be used to assess the accuracy of spike trains with less than 30 spikes (Holobar et al., 2014) or to assess the accuracy of each individual spike in a spike train.

Some information about accuracy can be obtained from the spike-triggered averaging of EMG signals (Del Vecchio and Farina, 2019; Hu et al., 2015, 2013b; Thompson et al., 2018). With this approach, the discharge times of identified motor units are used as triggers for an average that is accumulated over time intervals of 25 to 100 ms. Due to the possibility that motor unit action potential shapes change during an isometric contraction, a relatively small number of motor unit discharge times should be used in the spike-triggered average. We empirically observed that 3 s to 5 s (~30-100 spikes) are sufficient to robustly extract motor action potential waveforms during sustained and fast isometric contractions (A Del Vecchio et al., 2019c). Also, the reliability of an identified motor unit pool can be examined by identifying the same motor units across days (see *Motor unit Tracking)*.

6 – Assessment of motor unit properties

From the discharge times of identified motor units, the characteristics of the engaged motor units can be identified. One key characteristic is the recruitment threshold, which corresponds to the force when the first motor unit action potential occurs. The ensuing force that is produced by the muscle fibres innervated by the motoneuron (the muscle unit) occurs with a delay that depends on the axonal conduction velocity and on the properties (active and passive) of the muscle fibres. To obtain reliable estimates of recruitment and derecruitment thresholds, subjects must practice performing slow linear ramp contractions.

A common approach used to estimate recruitment threshold and to measure the discharge characteristics of motor units is the performance of trapezoidal force trajectories with controlled rates of increase and decrease in force (5-20% MVC/s) to a moderate plateau force (35-70% of maximal

force). Given the current limitations in HDEMG decomposition analysis in uniformly sampling motor units across recruitment thresholds, it is best practice to use a range of target forces (30 to 70-90% of maximum force) depending on the test muscle and type of contraction.

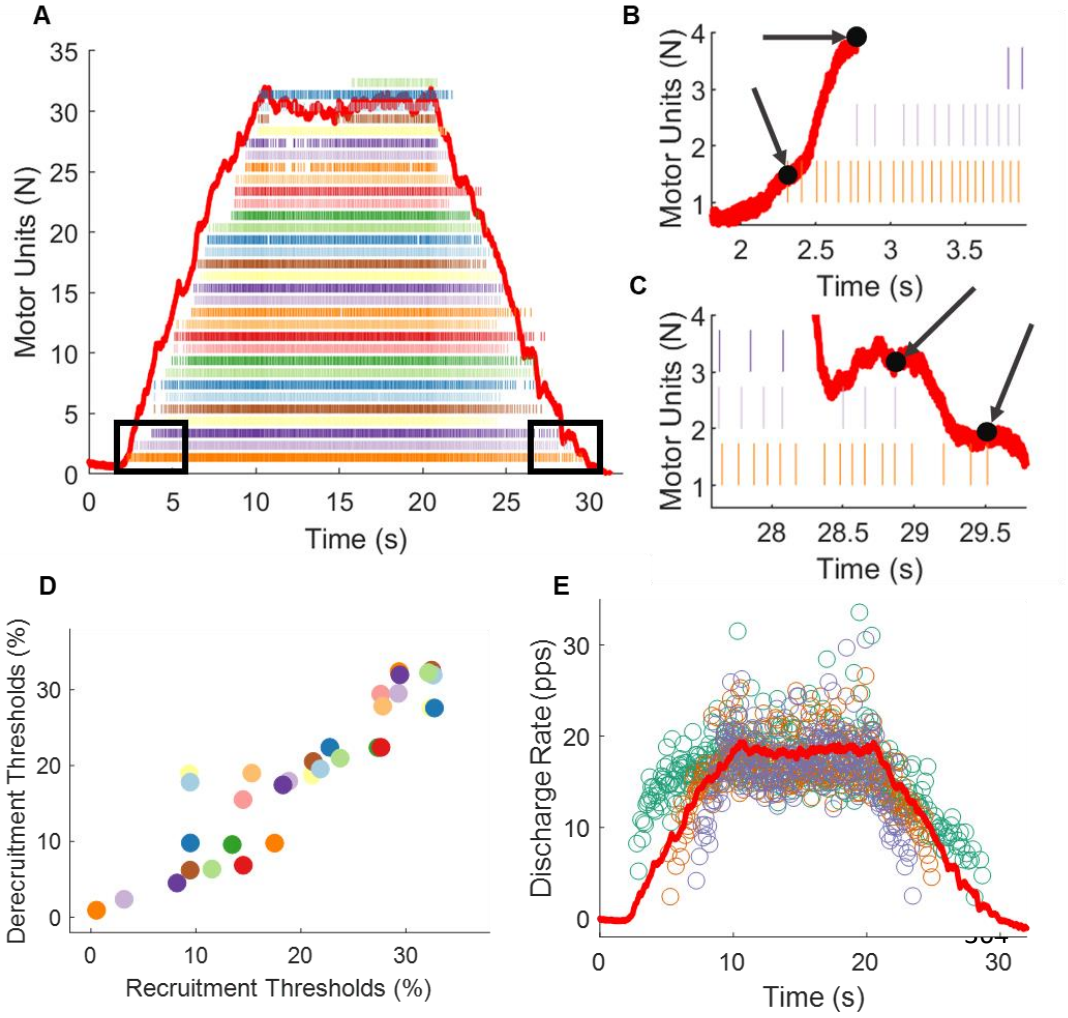

Figure 7. Motor unit properties: recruitment thresholds and discharge rates during an isometric trapezoidal contraction (plateau 35% of maximum). **A**. Raster plot of 32 identified motor units during an isometric contraction of the tibialis anterior muscle. The black boxes highlight the recruitment (**B**) and derecruitment (**C**) phases for three motor units with the specific force indicated with a black arrow. **D.** The association between recruitment threshold and derecruitment thresholds. **E**. The instantaneous discharge rate (the inverse of the interspike interval) as a function of time for the three representative motor units. The force trace is in red colour.

Figure 7 shows the raster plot of discharge times of 32 motor units during a trapezoidal contraction up to 35% of the maximum force of the tibialis anterior muscle. The recruitment and derecruitment thresholds are highlighted in Figure 7A-C. Once the interspike intervals are known, the motor unit discharge rates can be determined during the recruitment, plateau, and derecruitment phases, as shown in Figure 7E for three representative motor units.

Estimates of motor unit recruitment threshold during fast contractions can provide a measure of the speed of recruitment (Fig. 8).

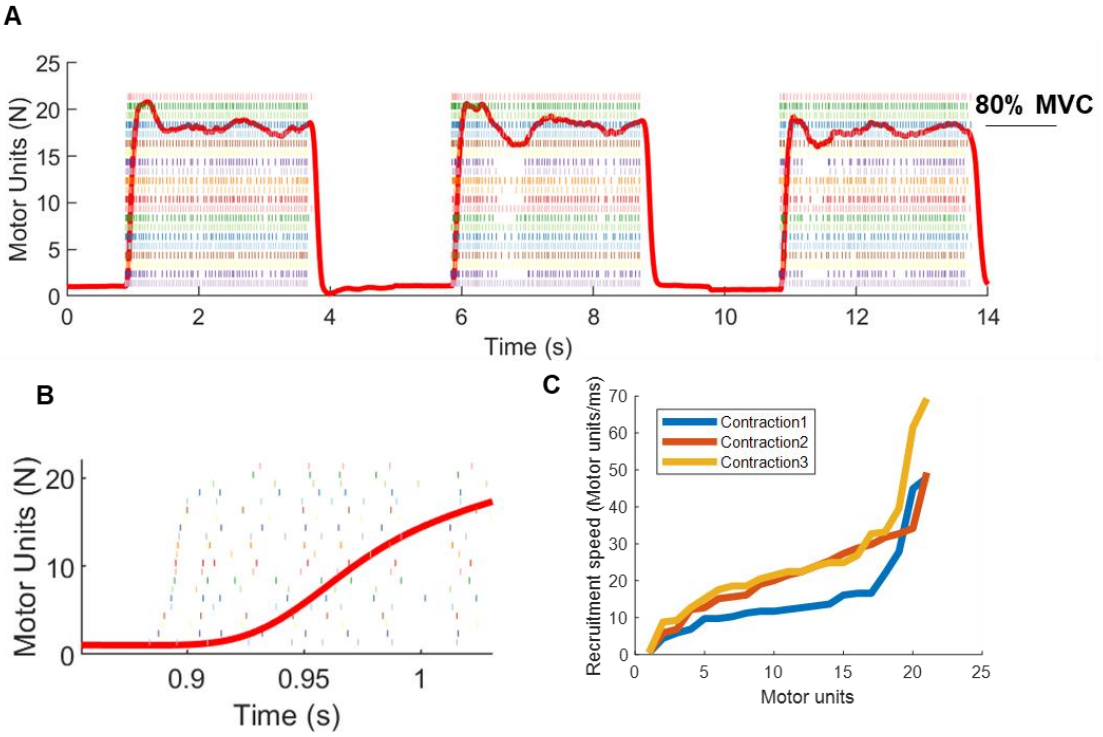

Figure 8 Motor unit recruitment during fast contractions. **A**. Three rapid isometric contractions of the tibialis anterior muscle. The plateau of the force is ~80% of maximum (red-trace). **B**. One representative contraction during the first 100 ms. The discharge times of identified motor units are shown as tick marks. **C**. Motor unit recruitment speed represents the time interval between the first discharge times of consecutive motor units (B). This value is calculated by taking the average of the derivative of the first discharge times of the motor unit pool (sorted by recruitment order). The x-axis label in C is sorted with respect to the motor units showing the smallest time interval. In this example, all the identified motor units were recruited in a small time window (<50 motor units/ms).

From the discharge times of the motor units, it is possible to extract characteristics of the common synaptic input to the motoneuron pool. These measures can be obtained in both the time and frequency domain. One time domain approach is to compute the cross-correlogram between motor unit discharges (Nordstrom et al., 1992). This method, originally proposed for pairs of motor units, can be extended to populations of motoneurons by summing the motor unit spike trains (binary signal) to generate the cumulative spike trains (CST). The cross-correlogram is then performed between the CSTs of randomly permuted groups of motor units (Figure 9). The rate of increase in correlation between CSTs when the number of motor units used for the CST calculation increases is associated to the relative proportion of common input with respect to independent input. This proportion can also be quantified by non-linear fitting of the peak correlation values in the frequency domain (Negro et al., 2016b), or in the time domain. These estimates provide information on a bandwidth of motor neuron input that depends on the filtering

of the CSTs. For example, by using a Hanning window of 25-ms (A Del Vecchio et al., 2019b), the analysed bandwidth is approximately 40 Hz.

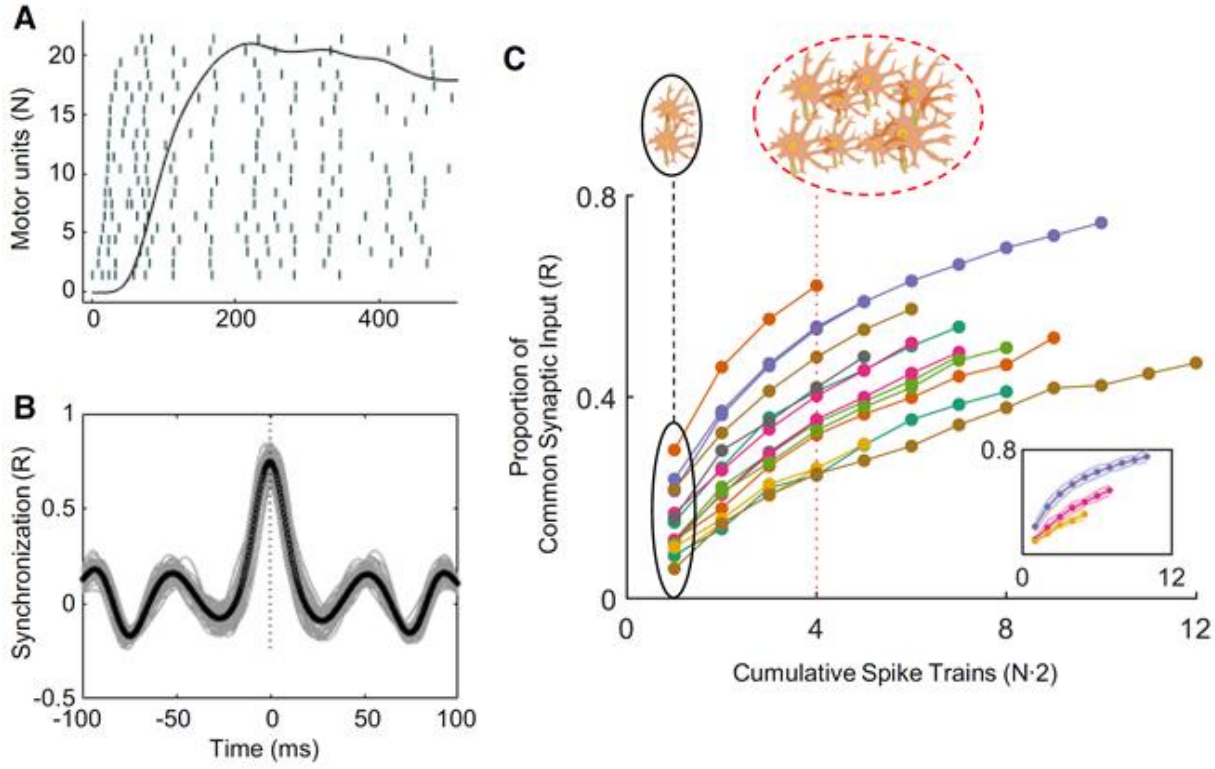

Figure 9. Calculation of the proportion of common input from the cross-correlogram. **A** Raster plot of 21 motor units during a fast contraction. **B** The cross-correlogram was obtained in 100-ms time windows with a 5-ms overlap. Each shaded grey line corresponds to a time window. For each calculation, the motor unit spike trains were divided in two equally sized groups and convolved with a 25-ms Hanning window. **C** Individual subject data (color-coded) for the strength of correlation between CSTs as a function of the number of motor units used for each CST. The inset in C shows three representative subjects with standard deviation across three rapid contractions (shaded colour). Modified from Del Vecchio et al. 2019 with permission.

It is further possible to estimate the frequency bands of the input shared by motoneurons (in the assumption of an approximate linear input-output relation for the motoneuron population) during steady contractions that last at least 20-30 s with the use of coherence functions. The coherence function provides a cross-correlation analysis in the frequency domain. Figure 10 shows the procedure for this calculation. Only motor unit spike trains without silent periods (>500 ms) should be included in this analysis. The coherence function can be also applied to study the shared synaptic inputs within the discharge timings of the populations of motoneurons. For this purpose, the coherence function is applied to groups of motor units that belong to different muscles, as described previously (Del Vecchio et al., 2019; Laine et al., 2015).

Another information that can be extracted from the motor unit discharge times is an estimate of the strength of persistent inward currents (PICs) to motoneurones from the discharge rates at recruitment

and derecruitment (Gorassini et al., 2002; Heckman et al., 2005). This measure reflects neuromodulatory input received by motoneurones and has been recently performed from HDEMG signal decomposition (Hassan et al., 2020).

From the shape of the motor unit action potential waveform it is also possible to extract other physiological information. This information includes analysis of the motor unit waveform, such as amplitude and conduction velocity (see paragraph 1-2 and Figure 2). The analysis of the motor unit discharge times and action potential waveforms enables the analysis of neural and peripheral properties concurrently. For example, the strong association between motor unit recruitment thresholds and motor unit conduction velocities that have been reported for different muscles (Andreassen and Arendt-Nielsen, 1987; Del Vecchio et al., 2018; Hogrel, 2003; Masuda and De Luca, 1991) is consistent with the size principle. Although in some cases this information has been used to infer the type of recruited (fast-twitch or slow twitch) muscle fibres, in-vivo studies show that there is no clustering of conduction velocity values but rather a continuous distribution of conduction velocities and estimated muscle fibre diameters (Del Vecchio et al., 2018; Troni et al., 1983), which agrees with basic physiological studies (see Enoka et al., 2015 for review).

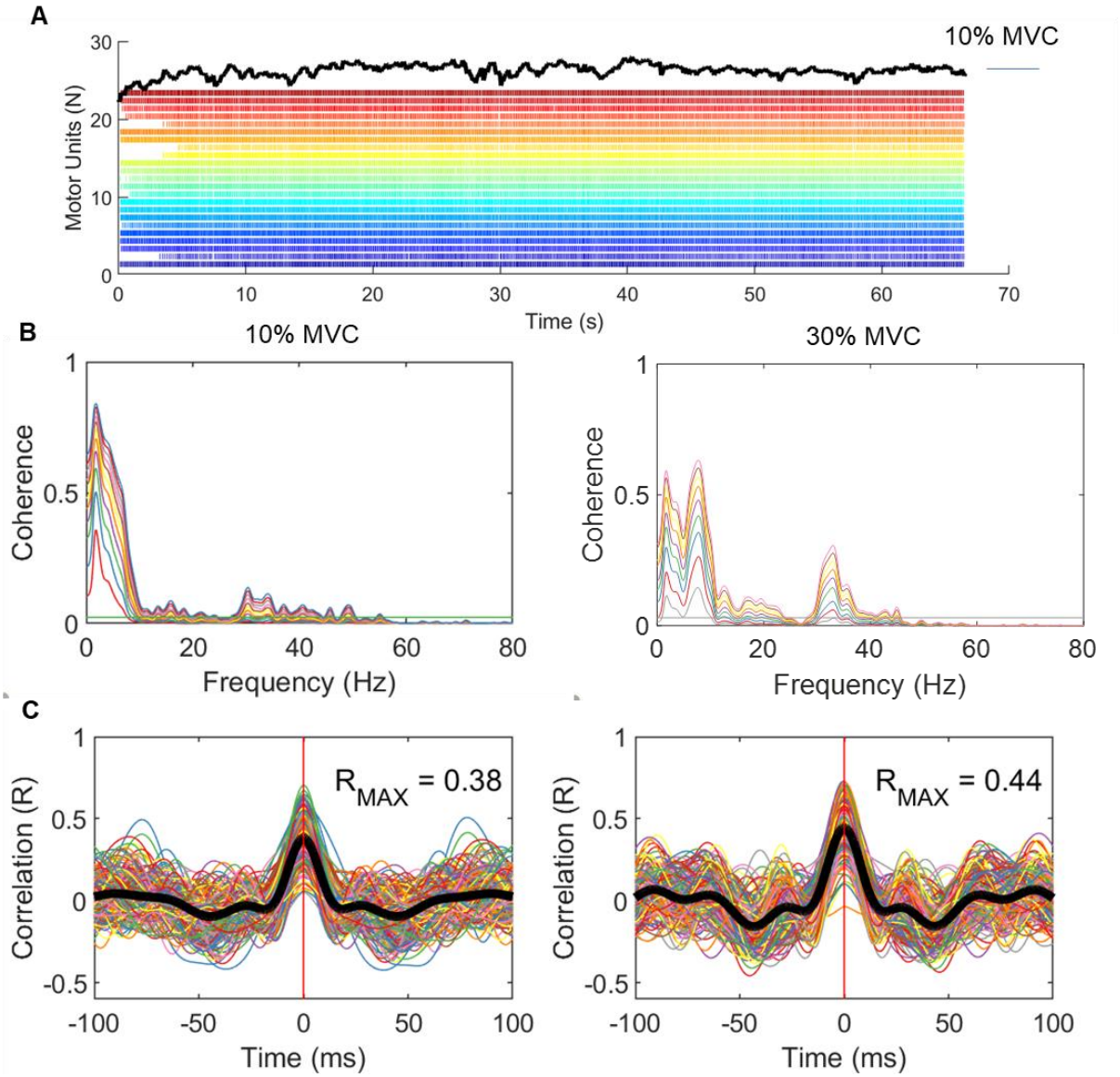

Figure 10 A. Raster plot of motor unit discharge times from the tibialis anterior muscle during a steady contraction at 10% of maximal voluntary force. **B.** The coherence function was calculated between increasing numbers of motor units (color coded) for a contraction at 10 and one at 30% of the maximum. Note that the increase in the number of motor units corresponds to an increase in the frequency coupling in all frequency bands above significance (the significant level was computed as the maximal value of coherence above 100 Hz). **C**. The correlation in the time domain obtained by the cross-correlogram in 100-ms windows.

7 - Motor unit tracking

The comparison of motor unit properties during longitudinal studies, such as after a rehabilitation intervention, is only possible if the same motor unit can be identified before and after the intervention. One advantage of HDEMG recordings is that they usually provide high spatial resolution of the motor unit action potentials. There is a small likelihood that two motor units would show exactly the same action potential waveforms in all channels for a large electrode grid (Farina et al., 2008), which means that motor units can be tracked over multiple sessions when the grid is placed in a similar location in each session (Del Vecchio and Farina, 2019; Martinez-Valdes et al., 2017).

Figure 11 shows an example of motor unit tracking during an isometric contraction with the ankle dorsiflexors. In this example, only some of the identified motor units could be tracked across experimental sessions. In our experience, approximately 30% of the identified units can be tracked over weeks in the tibialis anterior muscle. Motor unit tracking requires consistent placement of the high-density grid and the establishment of a threshold in cross-correlation between motor unit action potentials. When multiple motor units have a high cross-correlation between each other, which happens occasionally, these motor units should be removed from the tracking (see Figure 3 in (A Del Vecchio et al., 2019a)).

The motor unit tracking technique can also be used to test decomposition accuracy. Figure 11 shows two pools of motor units identified during two experimental sessions four weeks apart during isometric trapezoidal contractions of the tibialis anterior muscle. The action potential waveforms of these motor units were used to track the motor units over time (Fig 11B). Once the motor units are tracked, it is possible to test the accuracy and reliability of the discharge characteristics of the motor units, such as discharge rate and recruitment thresholds. Figure 11C-D shows that the tracked motor units exhibited strong reliability in discharge rate and recruitment threshold. It is important to note that the tracking technique uses the 2D action potential waveforms, therefore the physiological properties of the motor units are not taken into account during tracking. It is unlikely that a pool of motor units shows the same discharge characteristics across days (as demonstrated by comparing random motor units across sessions; Martinez-Valdes *et al.*, 2017) if the motor unit tracking and the initial decomposition were not performed correctly (Figure 11).

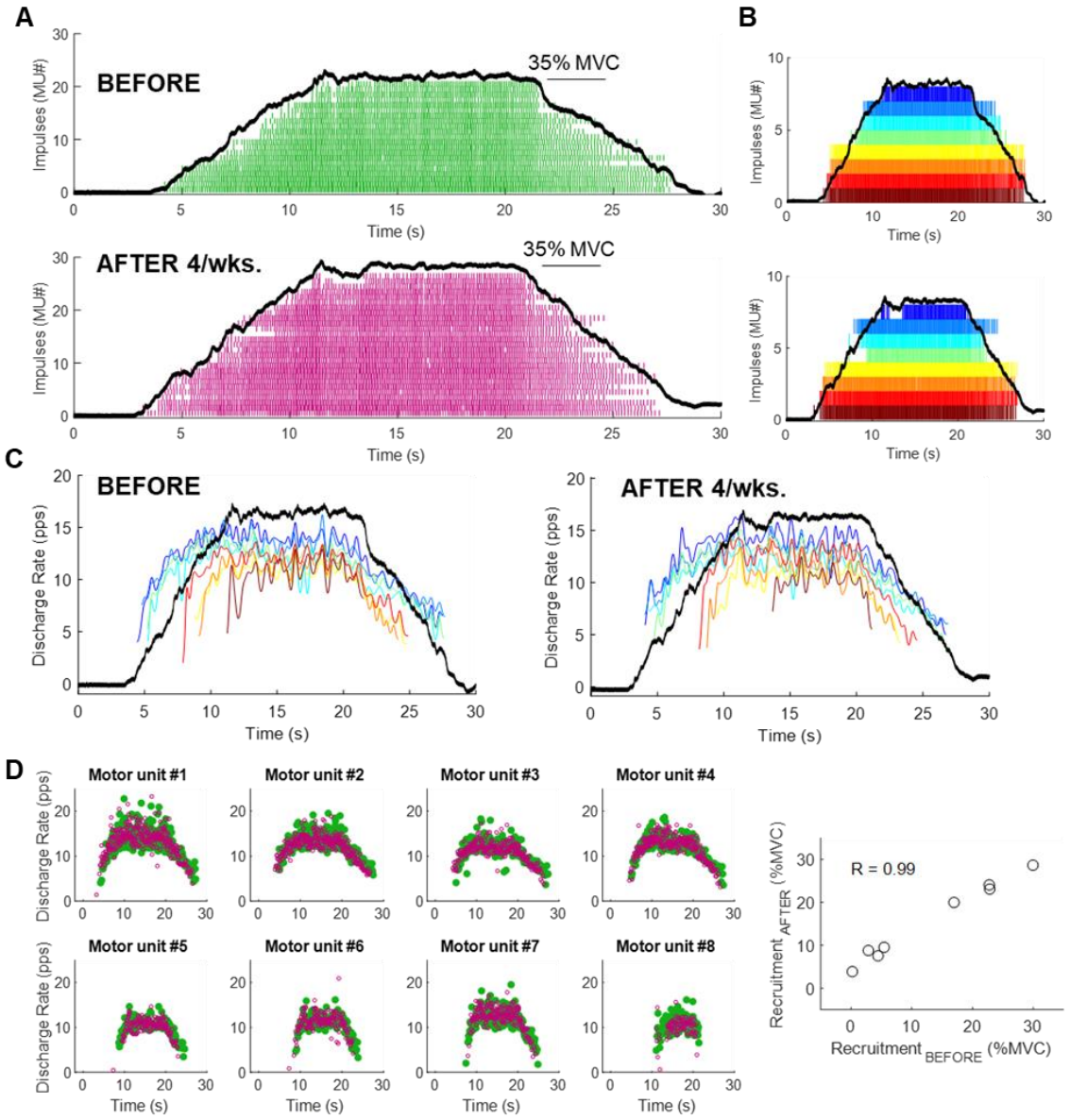

Figure 11. *Motor unit tracking.* One method that can be used to assess decomposition accuracy is to track the same motor unit across time. **A.** Two isometric contractions were performed by the same subject with 4 weeks between contractions. The number of identified motor units (green vs purple) differs in the two contractions. **B.** The same motor unit is tracked across time by matching the action potential waveforms**.** Eight motor units that were successfully tracked in the two contractions. Note the similar smoothed discharge rate (**C**), the instantaneous discharge rate (**D**), and the recruitment thresholds (the tracked motor units are color-coded). The scatter plot in **D** shows a strong correlation ($P<0.0001$) for recruitment thresholds before and after four weeks, thereby underscoring the accuracy in decomposition.

8 – Influencing factors in motor unit decomposition: the influence of muscle, volume conductor, and target force

There are three major limitations that limit the applicability of surface EMG decomposition in some experimental conditions. The output of the decomposition is sensitive to the muscles investigated, the volume conductor properties of the specific subject, and the contraction intensity. These limitations are due to anatomical constraints (the volume conductor between the recording electrodes and the muscle

481 units) and superimposition of the muscle fibre action potentials. With increasing contraction forces, the
482 number of motor units that can be identified by decomposition usually decreases. For example, in the
483 tibialis anterior muscle, which is a reliable muscle for decomposition (Del Vecchio and Farina, 2019;
484 Negro et al., 2016a), we observed a 30% reduction in the number of motor units that can be identified
485 when the target force increases from 35% to 70% of maximum force. Similarly, there is a trend for a
486 lower number of identified motor units for subjects with a thicker subcutaneous layer. These trends are
487 due to the decrease in discriminative information in the action potential waveforms of different motor
488 units when the signal bandwidth is reduced by the volume conductor (Farina et al., 2008). There are
489 still not sufficient data to reach a conclusion on the number of identified motor units between sexes.

490

491 Figure 12 shows the number of identified motor unit across muscles, sex, and contraction intensity for
492 a relatively large dataset of decomposed signals collected in the laboratories of the Authors. Some
493 muscles yield higher numbers of motor units irrespective of the contraction intensity (such as tibialis
494 anterior, see Fig 12). We have noted that muscles with fibres that are not all parallel to each other
495 usually yield a greater number of identified motor units by decomposition. This is likely due to the larger
496 discriminative information between motor unit action potentials of different units in muscles with varying
497 anatomy.

498

499

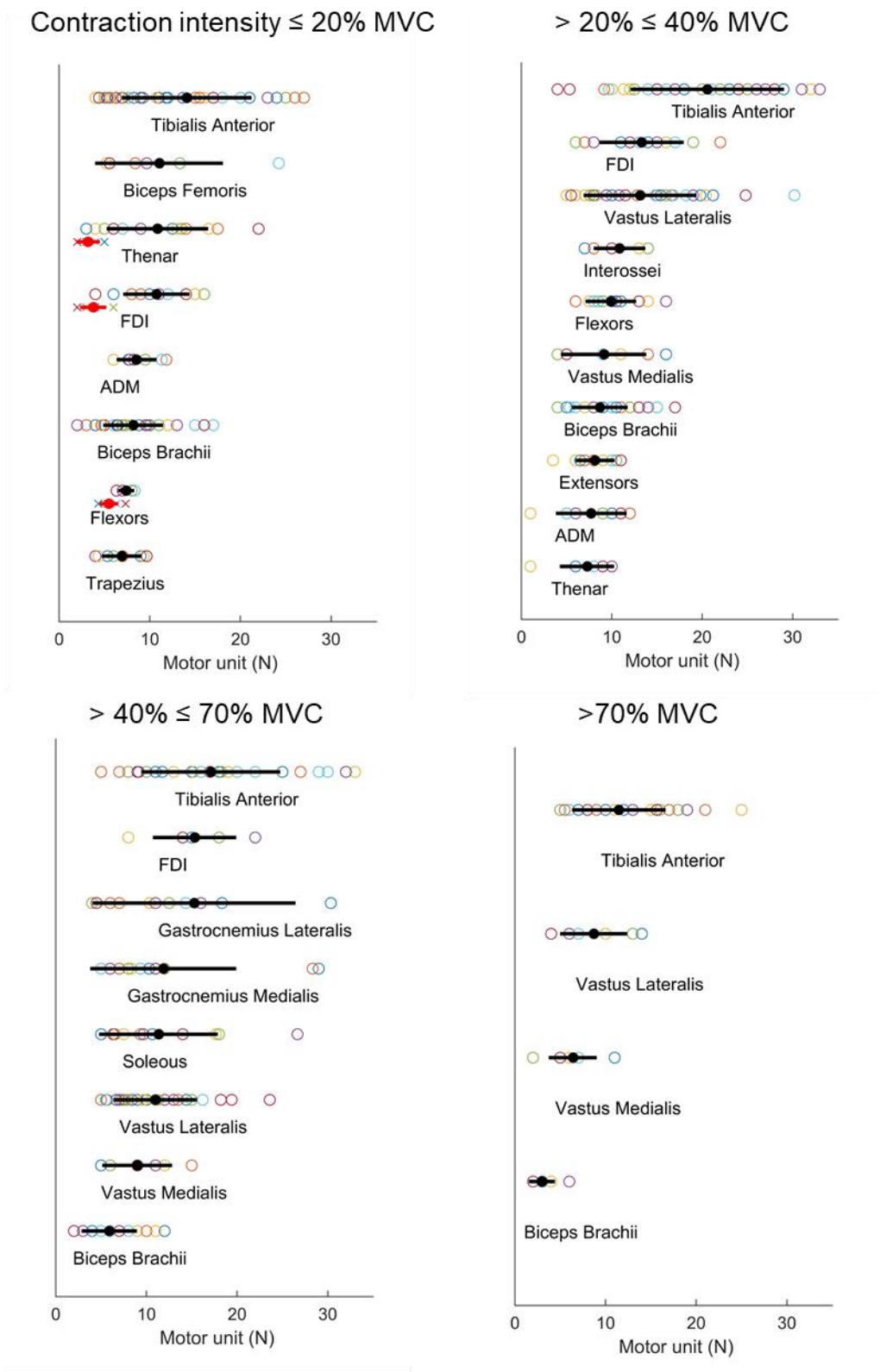

Figure 12 Number of identified motor units across muscles and contraction intensities. The average number (black dots) and standard deviation (black line) across subjects (color-coded), muscles, and contraction intensities. The red line and x dots for three muscles at ≤20% MVC indicate data for women. Note that some muscles yield a greater number of identified motor units irrespective of the contraction intensity. The data shown here are from recordings from the laboratories of the Authors. All the motor

units reported in this graph were decomposed with a pulse-to-noise ratio >30dB and were visually inspected as described in this tutorial.

Conclusions

In this tutorial we present guidelines for the extraction of motor unit discharge characteristics from HDEMG signals. This article provides an overview of the rationale for decomposition of EMG signals and then describes the step-to-step guidelines on how to perform an accurate decomposition, interpretation, and analysis of motor unit discharge times. Although the advances in software and hardware technology obtained in the last two decades potentially allows any experimenter to record motor units, there are many challenges that need to be overcome and many limitations that need to be solved thorough experimental testing and the development of additional software and hardware. We emphasise that the output of decomposition must be inspected carefully. Moreover, progress is still needed to improve surface EMG decomposition to reduce the limitations associated with variability of performance due to muscle and subject anatomy.

Acknowledgement

This study was supported by the European research Council Synergy project NaturalBionicS 810346), and by the Slovenian Research Agency (projects J2-1731 and L7-9421 and Programme funding P2-0041).

Reference

Andreassen, S., Arendt-Nielsen, L., 1987. Muscle fibre conduction velocity in motor units of the human anterior tibial muscle: a new size principle parameter. J. Physiol. 391, 561–571.

Barbero, M., Merletti, R., Rainoldi, A., 2012. Atlas of Muscle Innervation Zones, Atlas of Muscle Innervation Zones. https://doi.org/10.1007/978-88-470-2463-2

Besomi, M., Hodges, P.W., Van Dieën, J., Carson, R.G., Clancy, E.A., Disselhorst-Klug, C., Holobar, A., Hug, F., Kiernan, M.C., Lowery, M., McGill, K., Merletti, R., Perreault, E., Søgaard, K., Tucker, K., Besier, T., Enoka, R., Falla, D., Farina, D., Gandevia, S., Rothwell, J.C., Vicenzino, B., Wrigley, T., 2019. Consensus for experimental design in electromyography (CEDE) project: Electrode selection matrix. J. Electromyogr. Kinesiol. https://doi.org/10.1016/j.jelekin.2019.07.008

Casolo, A., Farina, D., Falla, D., Bazzucchi, I., Felici, F., Del Vecchio, A., 2019. Strength Training Increases Conduction Velocity of High-Threshold Motor Units. Med. Sci. Sport. Exerc. 1. https://doi.org/10.1249/MSS.0000000000002196

Chen, M., Zhang, X., Chen, X., Zhou, P., 2018. Automatic Implementation of Progressive FastICA Peel-Off for High Density Surface EMG Decomposition. IEEE Trans. Neural Syst. Rehabil. Eng. https://doi.org/10.1109/TNSRE.2017.2759664

Chen, M., Zhou, P., 2016. A novel framework based on FastICA for high density surface EMG decomposition. IEEE Trans. Neural Syst. Rehabil. Eng. 24, 117–127. https://doi.org/10.1109/TNSRE.2015.2412038

Day, S.J., Hulliger, M., 2001. Experimental simulation of cat electromyogram: Evidence for algebraic summation of motor-unit action-potential trains. J. Neurophysiol. 86, 2144–2158.

De Luca, C.J., Adam, A., Wotiz, R., Gilmore, L.D., Nawab, S.H., 2006. Decomposition of surface EMG signals. J. Neurophysiol. https://doi.org/10.1152/jn.00009.2006

549 Del Vecchio, A, Casolo, A., Negro, F., Scorcelletti, M., Bazzucchi, I., Enoka, R., Felici, F., Farina, D.,
550 2019a. The increase in muscle force after 4 weeks of strength training is mediated by
551 adaptations in motor unit recruitment and rate coding. J. Physiol. 0, JP277250.
552 https://doi.org/10.1113/JP277250

553 Del Vecchio, A, Falla, D., Felici, F., Farina, D., 2019b. The relative strength of common synaptic input
554 to motor neurons is not a determinant of the maximal rate of force development in humans. J.
555 Appl. Physiol. 127, 205–214. https://doi.org/10.1152/japplphysiol.00139.2019

556 Del Vecchio, A., Farina, D., 2019. Interfacing the neural output of the spinal cord: robust and reliable
557 longitudinal identification of motor neurons in humans. J. Neural Eng. 17, 016003.
558 https://doi.org/10.1088/1741-2552/ab4d05

559 Del Vecchio, A., Germer, C.M., Elias, L.A., Fu, Q., Fine, J., Santello, M., Farina, D., 2019. The human
560 central nervous system transmits common synaptic inputs to distinct motor neuron pools during
561 non-synergistic digit actions. J. Physiol. 597, 5935–5948. https://doi.org/10.1113/JP278623

562 Del Vecchio, A., Negro, F., Felici, F., Farina, D., 2018. Distribution of muscle fibre conduction velocity
563 for representative samples of motor units in the full recruitment range of the tibialis anterior
564 muscle. Acta Physiol. 222, e12930. https://doi.org/10.1111/apha.12930

565 Del Vecchio, A., Negro, F., Felici, F., Farina, D., 2017. Associations between motor unit action
566 potential parameters and surface EMG features. J. Appl. Physiol. 123, 835–843.
567 https://doi.org/10.1152/japplphysiol.00482.2017

568 Del Vecchio, A, Negro, F., Holobar, A., Casolo, A., Folland, J.P., Felici, F., Farina, D., 2019c. You are
569 as fast as your motor neurons: speed of recruitment and maximal discharge of motor neurons
570 determine the maximal rate of force development in humans. J. Physiol. 1–27.
571 https://doi.org/10.1113/JP277396

572 Del Vecchio, A, Ubeda, A., Sartori, M., Azorin, J.M., Felici, F., Farina, D., 2018. Central Nervous
573 System Modulates the Neuromechanical Delay in a Broad Range for the Control of Muscle
574 Force. J. Appl. Physiol. 44, japplphysiol.00135.2018.
575 https://doi.org/10.1152/japplphysiol.00135.2018

576 Desmedt, J.E., Godaux, E., 1977. Fast motor units are not preferentially activated in rapid voluntary
577 contractions in man. Nature 267, 717–9. https://doi.org/10.1038/267717a0

578 Dideriksen, J.L., Enoka, R.M., Farina, D., 2011. Neuromuscular adjustments that constrain
579 submaximal EMG amplitude at task failure of sustained isometric contractions. J. Appl. Physiol.
580 111, 485–494. https://doi.org/10.1152/japplphysiol.00186.2011

581 Dimitrov, G. V., Dimitrova, N.A., 1974. Extracellular potential field of a single striated muscle fibre
582 immersed in anisotropic volume conductor. Electromyogr. Clin. Neurophysiol.

583 Drost, G., Blok, J.H., Stegeman, D.F., van Dijk, J.P., van Engelen, B.G.M., Zwarts, M.J., 2001.
584 Propagation disturbance of motor unit action potentials during transient paresis in generalized
585 myotonia: A high-density surface EMG study. Brain 124, 352–360.
586 https://doi.org/10.1093/brain/124.2.352

587 Duchateau, J., Enoka, R.M., 2011. Human motor unit recordings: Origins and insight into the
588 integrated motor system. Brain Res. 1409, 42–61. https://doi.org/10.1016/j.brainres.2011.06.011

589 Enoka, R.M., 2019. Physiological Validation of the Decomposition of Surface EMG Signals. J.
590 Electromyogr. Kinesiol. https://doi.org/10.1016/j.jelekin.2019.03.010

591 Enoka, R.M., Duchateau, J., 2015. Inappropriate interpretation of surface EMG signals and muscle
592 fiber characteristics impedes understanding of the control of neuromuscular function. J. Appl.
593 Physiol. 119, 1516–1518. https://doi.org/10.1152/japplphysiol.00280.2015

594 Farina, D., Arendt-Nielsen, L., Merletti, R., Graven-Nielsen, T., 2002a. Assessment of single motor
595 unit conduction velocity during sustained contractions of the tibialis anterior muscle with
596 advanced spike triggered averaging. J. Neurosci. Methods 115, 1–12.
597 https://doi.org/10.1016/S0165-0270(01)00510-6

598 Farina, D., Fosci, M., Merletti, R., 2002b. Motor unit recruitment strategies investigated by surface
599 EMG variables. J. Appl. Physiol. 92, 235–247. https://doi.org/11744666

600 Farina, D., Holobar, A., Merletti, R., Enoka, R.M., 2010. Decoding the neural drive to muscles from
601 the surface electromyogram. Clin. Neurophysiol. 121, 1616–1623.
602 https://doi.org/10.1016/j.clinph.2009.10.040

603 Farina, D., Merletti, R., Enoka, R.M., 2014. The extraction of neural strategies from the surface EMG:
604 an update. J. Appl. Physiol. 117, 1215–1230. https://doi.org/10.1152/japplphysiol.01070.2003

605 Farina, D., Merletti, R., Enoka, R.M., 2004. The extraction of neural strategies from the surface EMG.
606 J. Appl. Physiol. 96, 1486–1495. https://doi.org/10.1152/japplphysiol.01070.2003

607 Farina, D., Negro, F., Gazzoni, M., Enoka, R.M., 2008. Detecting the unique representation of motor-
608 unit action potentials in the surface electromyogram. J. Neurophysiol.
609 https://doi.org/10.1152/jn.90219.2008

610 Feeney, D.F., Mani, D., Enoka, R.M., 2018. Variability in common synaptic input to motor neurons
611 modulates both force steadiness and pegboard time in young and older adults. J. Physiol. 596,
612 3793–3806. https://doi.org/10.1113/JP275658

613 Fuglevand, A.J., Winter, D.A., Patla, A.E., 1993. Models of recruitment and rate coding organization in
614 motor-unit pools. J. Neurophysiol. 70, 2470–2488.

615 Fuglevand, A.J., Winter, D.A., Patla, A.E., Stashuk, D., 1992. Detection of motor unit action potentials
616 with surface electrodes: influence of electrode size and spacing. Biol. Cybern.
617 https://doi.org/10.1007/BF00201021

618 Gallego, J.A., Dideriksen, J.L., Holobar, A., Ibanez, J., Glaser, V., Romero, J.P., Benito-Leon, J.,
619 Pons, J.L., Rocon, E., Farina, D., 2015. The Phase Difference Between Neural Drives to
620 Antagonist Muscles in Essential Tremor Is Associated with the Relative Strength of Supraspinal
621 and Afferent Input. J. Neurosci. 35, 8925–8937. https://doi.org/10.1523/JNEUROSCI.0106-
622 15.2015

623 Gandevia, S.C., Macefield, G., Burke, D., Mckenzie, D.K., 1990. Voluntary activation of human motor
624 axons in the absence of muscle afferent feedback: The control of the deafferented hand. Brain
625 113, 1563–1581. https://doi.org/10.1093/brain/113.5.1563

626 Gazzoni, M., Camelia, F., Farina, D., 2005. Conduction velocity of quiscent muscle fibers decreases
627 during sustained contraction. J. Neurophysiol. 94, 387–394.
628 https://doi.org/10.1152/jn.01182.2004.

629 Gazzoni, M., Farina, D., Merletti, R., 2004. A new method for the extraction and classification of single
630 motor unit action potentials from surface EMG signals. J. Neurosci. Methods.
631 https://doi.org/10.1016/j.jneumeth.2004.01.002

632 Gorassini, M., Yang, J.F., Siu, M., Bennett, D.J., 2002. Intrinsic activation of human motoneurons:
633 reduction of motor unit recruitment thresholds by repeated contractions. J. Neurophysiol. 87,
634 1859–1866. https://doi.org/10.1152/jn.00025.2001

635 Håkansson, C.H., 1956. Conduction Velocity and Amplitude of the Action Potential as Related to
636 Circumference in the Isolated Fibre of Frog Muscle. Acta Physiol. Scand. 37, 14–34.
637 https://doi.org/10.1111/j.1748-1716.1956.tb01338.x

638 Hassan, A., Thompson, C.K., Negro, F., Cummings, M., Powers, R.K., Heckman, C.J., Dewald,
639 J.P.A., McPherson, L.M., 2020. Impact of parameter selection on estimates of motoneuron
640 excitability using paired motor unit analysis, in: Journal of Neural Engineering.
641 https://doi.org/10.1088/1741-2552/ab5eda

642 Heckman, C.J., Enoka, R.M., 2012. Motor Unit. Compr. Physiol. 2, 2629–2682.
643 https://doi.org/10.1002/cphy.c100087

644 Heckman, C.J., Gorassini, M.A., Bennett, D.J., 2005. Persistent inward currents in motoneuron
645 dendrites: Implications for motor output. Muscle and Nerve 31, 135–156.
646 https://doi.org/10.1002/mus.20261

Henneman, E., Somjen, G., Carpenter, D.O., 1965. Functional Significance of Cell Size in Spinal Motoneurons. J. Neurophysiol. 28, 560–580.

Hogrel, J.Y., 2003. Use of surface EMG for studying motor unit recruitment during isometric linear force ramp. J. Electromyogr. Kinesiol. 13, 417–423. https://doi.org/10.1016/S1050-6411(03)00026-9

Holobar, A., Minetto, M.A., Botter, A., Negro, F., Farina, D., 2010. Experimental analysis of accuracy in the identification of motor unit spike trains from high-density surface EMG. IEEE Trans. Neural Syst. Rehabil. Eng. 18, 221–229. https://doi.org/10.1109/TNSRE.2010.2041593

Holobar, A., Minetto, M.A., Farina, D., 2014. Accurate identification of motor unit discharge patterns from high-density surface EMG and validation with a novel signal-based performance metric. J. Neural Eng. 11, 016008. https://doi.org/10.1088/1741-2560/11/1/016008

Holobar, A., Zazula, D., 2007. Multichannel blind source separation using convolution Kernel compensation. IEEE Trans. Signal Process. 55, 4487–4496. https://doi.org/10.1109/TSP.2007.896108

Hu, X., Rymer, W.Z., Suresh, N.L., 2014. Motor unit firing rate patterns during voluntary muscle force generation: a simulation study. J. Neural Eng. 11, 26015. https://doi.org/10.1088/1741-2560/11/2/026015

Hu, X., Rymer, W.Z., Suresh, N.L., 2013a. Motor unit pool organization examined via spike-triggered averaging of the surface electromyogram. J. Neurophysiol. 110, 1205–20. https://doi.org/10.1152/jn.00301.2012

Hu, X., Rymer, W.Z., Suresh, N.L., 2013b. Assessment of validity of a high-yield surface electromyogram decomposition. J. Neuroeng. Rehabil. 10, 1. https://doi.org/10.1186/1743-0003-10-99

Hu, X., Suresh, A.K., Rymer, W.Z., Suresh, N.L., 2015. Assessing altered motor unit recruitment patterns in paretic muscles of stroke survivors using surface electromyography. J. Neural Eng. 12, 66001. https://doi.org/10.1088/1741-2560/12/6/066001

Keenan, K.G., Farina, D., Merletti, R., Enoka, R.M., 2006. Amplitude cancellation reduces the size of motor unit potentials averaged from the surface EMG. J Appl Physiol 100, 1928–1937. https://doi.org/10.1152/japplphysiol.01282.2005

Komi, P. V., Viitasalo, J.H.T., 1976. Signal Characteristics of EMG at Different Levels of Muscle Tension. Acta Physiol. Scand. 96, 267–276. https://doi.org/10.1111/j.1748-1716.1976.tb10195.x

Kumar, R.I., Mallette, M.M., Cheung, S.S., Stashuk, D.W., Gabriel, D.A., 2020. A method for editing motor unit potential trains obtained by decomposition of surface electromyographic signals. J. Electromyogr. Kinesiol. 50, 102383. https://doi.org/10.1016/j.jelekin.2019.102383

Laine, C.M., Martinez-Valdes, E., Falla, D., Mayer, F., Farina, D., 2015. Motor Neuron Pools of Synergistic Thigh Muscles Share Most of Their Synaptic Input. J. Neurosci. 35, 12207–12216. https://doi.org/10.1523/JNEUROSCI.0240-15.2015

LeFever, R.S., De Luca, C.J., 1982. A Procedure for Decomposing the Myoelectric Signal Into Its Constituent Action Potentials— Part I: Technique, Theory, and Implementation. IEEE Trans. Biomed. Eng. https://doi.org/10.1109/TBME.1982.324881

LeFever, R.S., Xenakis, A.P., De Luca, C.J., 1982. A Procedure for Decomposing the Myoelectric Signal Into Its Constituent Action Potentials— Part II; Execution and Test for Accuracy. IEEE Trans. Biomed. Eng. https://doi.org/10.1109/TBME.1982.324882

Mambrito, B., De Luca, C.J., 1984. A technique for the detection, decomposition and analysis of the EMG signal. Electroencephalogr. Clin. Neurophysiol. 58, 175–188. https://doi.org/10.1016/0013-4694(84)90031-2

Mañanas, M.A., Rojas-Martínez, M., Alonso, J.F., 2016. Towards the application of HD-EMG decomposition in clinical practice. Clin. Neurophysiol. 127, 2532–2533. https://doi.org/10.1016/j.clinph.2016.02.005

696 Marateb, H.R., McGill, K.C., Holobar, A., Lateva, Z.C., Mansourian, M., Merletti, R., 2011. Accuracy
697 assessment of CKC high-density surface EMG decomposition in biceps femoris muscle. J.
698 Neural Eng. 8. https://doi.org/10.1088/1741-2560/8/6/066002

699 Martinez-Valdes, E., Farina, D., Negro, F., Del Vecchio, A., Falla, D., 2018. Early Motor Unit
700 Conduction Velocity Changes to High-Intensity Interval Training versus Continuous Training.
701 Med. Sci. Sports Exerc. 50, 2339–2350. https://doi.org/10.1249/MSS.0000000000001705

702 Martinez-Valdes, E., Negro, F., Laine, C.M., Falla, D., Mayer, F., Farina, D., 2017. Tracking motor
703 units longitudinally across experimental sessions with high-density surface electromyography. J.
704 Physiol. 595, 1479–1496. https://doi.org/10.1113/JP273662

705 Masuda, T., De Luca, C.J., 1991. Recruitment threshold and muscle fiber conduction velocity of single
706 motor units. J. Electromyogr. Kinesiol. 1, 116–123. https://doi.org/10.1016/1050-6411(91)90005-
707 P

708 Masuda, T., Sadoyama, T., Shiraishi, M., 1996. Dependence of average muscle fibre conduction
709 velocity on voluntary contraction force. J. Electromyogr. Kinesiol. 6, 267–276.
710 https://doi.org/10.1016/S1050-6411(96)00022-3

711 McGill, K.C., Lateva, Z.C., Marateb, H.R., 2005. EMGLAB: An interactive EMG decomposition
712 program. J. Neurosci. Methods 149, 121–133.

713 Merletti, R., Farina, D., 2016. Surface Electromyography: Physiology, Engineering and Applications,
714 Surface Electromyography: Physiology, Engineering and Applications.
715 https://doi.org/10.1002/9781119082934

716 Merletti, R., Farina, D., Gazzoni, M., 2003. The linear electrode array: A useful tool with many
717 applications. J. Electromyogr. Kinesiol. 13, 37–47. https://doi.org/10.1016/S1050-
718 6411(02)00082-2

719 Merletti, R., Farina, D., Granata, A., 1999. Non-invasive assessment of motor unit properties with
720 linear electrode arrays. Electroencephalogr. Clin. Neurophysiol. Suppl. 50, 293–300.

721 Merletti, R., Holobar, A., Farina, D., 2008. Analysis of motor units with high-density surface
722 electromyography. J. Electromyogr. Kinesiol. 18, 879–890.
723 https://doi.org/10.1016/j.jelekin.2008.09.002

724 Merletti, R., Muceli, S., 2019. Tutorial. Surface EMG detection in space and time: Best practices. J.
725 Electromyogr. Kinesiol. 49, 102363. https://doi.org/10.1016/j.jelekin.2019.102363

726 Milner-Brown, H.S., Stein, R.B., 1975. The relation between the surface electromyogram and
727 muscular force. J. Physiol. 246, 549–569. https://doi.org/10.1113/jphysiol.1975.sp010904

728 Milner-Brown, H.S., Stein, R.B., Yemm, R., 1973. The contractile properties of human motor units
729 during voluntary isometric contractions. J. Physiol. 228, 285–306.
730 https://doi.org/10.1113/jphysiol.1973.sp010087

731 Nawab, S.H., Chang, S.S., De Luca, C.J., 2010. High-yield decomposition of surface EMG signals.
732 Clin. Neurophysiol. 121, 1602–1615. https://doi.org/10.1016/j.clinph.2009.11.092

733 Negro, F., Muceli, S., Castronovo, A.M., Holobar, A., Farina, D., 2016a. Multi-channel intramuscular
734 and surface EMG decomposition by convolutive blind source separation. J. Neural Eng. 13,
735 026027. https://doi.org/10.1088/1741-2560/13/2/026027

736 Negro, F., Şükrü Yavuz, U., Farina, D., 2016b. The human motor neuron pools receive a dominant
737 slow-varying common synaptic input. J. Physiol. 0, 1–45. https://doi.org/10.1113/JP271748

738 Nordstrom, M.A., Fuglevand, A.J., Enoka, R.M., 1992. Estimating the strength of common input to
739 human motoneurons from the cross-correlogram. J. Physiol. 453, 547–74.
740 https://doi.org/10.1111/j.1365-2222.2007.02706.x

741 Piervirgili, G., Petracca, F., Merletti, R., 2014. A new method to assess skin treatments for lowering
742 the impedance and noise of individual gelled Ag-AgCl electrodes. Physiol. Meas.
743 https://doi.org/10.1088/0967-3334/35/10/2101

744 Plonsey, R., Barr, R.C., 1988. Bioelectricity: A quantitative Approach, Bioelectricity: A Quantitative
745 Approach. Springer Science & Business Media, New York, NY. https://doi.org/10.1007/978-0-
746 387-48865-3

747 Stashuk, D., de Bruin, H., 1988. Automatic Decomposition of Selective Needle-Detected Myoelectric
748 Signals. IEEE Trans. Biomed. Eng. https://doi.org/10.1109/10.1330

749 Stegeman, D.F., Dumitru, D., King, J.C., Roeleveld, K., 1997. Near- and far-fields: Source
750 characteristics and the conducting medium in neurophysiology. J. Clin. Neurophysiol.
751 https://doi.org/10.1097/00004691-199709000-00009

752 Thompson, C.K., Negro, F., Johnson, M.D., Holmes, M.R., McPherson, L.M., Powers, R.K., Farina,
753 D., Heckman, C.J., 2018. Robust and accurate decoding of motoneuron behaviour and
754 prediction of the resulting force output. J. Physiol. 0, 1–5. https://doi.org/10.1113/JP276153

755 Troni, W., Cantello, R., Rainero, I., 1983. Conduction velocity along human muscle fibers in situ.
756 Neurology 33, 1453–1459. https://doi.org/10.1212/WNL.33.11.1453

757 Zwarts, M.J., Arendt-Nielsen, L., 1988. The influence of force and circulation on average muscle fibre
758 conduction velocity during local muscle fatigue. Eur. J. Appl. Physiol. Occup. Physiol. 58, 278–
759 283. https://doi.org/10.1007/BF00417263

760 Zwarts, M.J., Stegeman, D.F., 2003. Multichannel surface EMG: Basic aspects and clinical utility.
761 Muscle and Nerve 28, 1–17. https://doi.org/10.1002/mus.10358

762